Ocean Sci. Discuss., 9, 3191–3238, 2012
www.ocean-sci-discuss.net/9/3191/2012/
doi:10.5194/osd-9-3191-2012

Ocean Science Discussions

Chaotic variability of the meridional overturning circulation on subannual to interannual timescales

J. J.-M. Hirschi[1], A. T. Blaker[1], B. Sinha[1], A. Coward[1], B. de Cuevas[1], S. Alderson[1], and G. Madec[1,2]

[1]National Oceanography Centre, Southampton, Southampton, SO14 3ZH, UK
[2]LOCEAN (CNRS/IRD/UPMC/MNHN) Institut Pierre et Simon Laplace, Paris, France

Received: 2 July 2012 – Accepted: 28 July 2012 – Published: 12 October 2012

Correspondence to: J. J.-M. Hirschi (jjmh@noc.soton.ac.uk)

Published by Copernicus Publications on behalf of the European Geosciences Union.

Abstract

Observations and numerical simulations have shown that the meridional overturning circulation (MOC) exhibits substantial variability on sub- to interannual timescales. This variability is not fully understood. In particular it is not known what fraction of the MOC variability is caused by processes such as mesoscale ocean eddies and internal waves which are ubiquitous in the ocean. Here we analyse twin experiments performed with a global ocean model at eddying (1/4°) and non-eddying (1°) resolutions. The twin experiments are forced with the same surface fluxes for the 1958 to 2001 period but start from different initial conditions. Our results show that on subannual to interannual timescales a large fraction of MOC variability directly reflects variability in the surface forcing. Nevertheless, in the eddy-permitting case there is an initial condition dependent MOC variability (hereinafter referred to as "chaotic" variability) of several Sv (1 Sv = 10^6 m^3 s^{-1}) in the Atlantic and the Indo-Pacific. In the Atlantic the chaotic MOC variability represents up to 30 % of the total variability at the depths where the maximum MOC occurs. In comparison the chaotic MOC variability is only 5–10 % in the non-eddying case. The surface forcing being identical in the twin experiments suggests that mesoscale ocean eddies are the most likely cause for the increased chaotic MOC variability in the eddying case. The exact formation time of eddies is determined by the initial conditions which are different in the two accordance with and as a consequence the mesoscale eddy field is decorrelated in the twin experiments. In regions where eddy activity is high in the eddy-permitting model, the correlation of sea surface height variability in the twin runs is close to zero. In the non-eddying case in contrast, we find high correlations (0.9 or higher) over most regions. Looking at the sub- and interannual MOC components separately reveals that despite the amplitude of the chaotic variability being larger on subannual than on interannual timescales, the ratio of chaotic to total MOC variability is larger on interannual than on subannual timescales.

OSD

9, 3191–3238, 2012

1 Introduction

Climate variability consists of both predictable and unpredictable (chaotic) components. Examples of predictable variability in the climate system are the diurnal cycle occurring as the Earth spins around its axis or the seasonal cycle, which is a consequence of the inclination of the Earth's axis with respect to the Ecliptic. Seasonal changes in temperature, precipitation and wind give rise to the known sequence of the seasons which shape the climate of the different regions of the Globe. An example of predictable variability on much longer timescales is the timing of the multimillennial ice age cycles which have characterised the Earth's climate for the last 2 Ma. The timing of the ice age cycles are given by changes in radiative forcing due to periodically changing parameters in the Earth's orbit around the sun (Imbrie et al., 1992; Bradley, 1985). Finally, another prominent example of climatic variability that also contains predictability on longer timescales (multi-decadal or longer) are the climate changes occurring in response to the emission of anthropogenic greenhouse gases into the atmosphere. Even though the debate about the amplitude of these changes and about their regional imprint is still ongoing, the basic physical mechanisms responsible for the greenhouse effect are well understood, which makes global climate change likely to be at least partly predictable.

In the examples of natural predictable climate variability given above the forcing is external (variations in insolation). However, despite the high predictability of this external forcing, the diurnal, seasonal and ice age cycles are also modulated by the internal variability of the climate system. The amplitude of the diurnal cycle for example depends on the weather. Similarly, seasons are affected by the prevailing state of the atmospheric circulation and despite the external forcing (insolation) typically being very similar from year to year, there is a large variability when the same season is compared between different years, e.g. at a given location a cold and dry winter in one at year may be followed by a mild and wet one the following year.

OSD
9, 3191–3238, 2012

The daily weather is probably the best known example of internal, unpredictable (chaotic) variability in the climate system. Even with the increasing wealth of observations available to define the initial conditions and contrain solutions in forecasting models, skilful forecasts are typically not possible for periods of more than 10 days and the reliability of forecasts rapidly drops after a few days. Events such as the onset and termination of blocking events in the atmosphere (linked to prolonged cold/warm, wet/dry conditions) are also largely unpredictable on timescales longer than a few days. In some instances there can be some early warning signs that a mode of variability could be in a certain state in a coming season (e.g. the North Atlantic Oscillation (NAO), Czaja and Frankignoul, 2002) but nevertheless, reliable seasonal forecasts tend to be elusive for many parts of the globe. Successful seasonal forecasts can be made for the El Niño Southern Oscillation (ENSO) which tends to occur every 2 to 7 years. Changes in tropical Pacific subsurface ocean temperature observed by the TOGA-TAO system can detect a coming El Niño event up to six months in advance (McPhaden, 1999). However, rather than actually predicting an ENSO event, the TOGA-TAO system picks up the very early stages of ENSO by monitoring changes in subsurface temperatures months before they become visible at the surface. Even with the TOGA-TAO observing system in the Pacific and the most advanced numerical models we cannot predict the onset of an ENSO event years in advance.

In the same way as the diurnal cycle or seasons are shaped by both external forcing and internal processes, the ocean circulation consists of components that can readily be explained and predicted from the action of the atmosphere on the ocean surface and an internal ("chaotic") variability. Examples of ocean circulation features that can be predicted from the wind, heat and freshwater forcings are the shape and position of ocean gyres with their intensified western boundary currents, the Antarctic Circumpolar Current, or seasonally varying currents e.g. in the Equatorial regions or driven by seasonal up- and downwelling along continental west coasts in the subtropics. However, the ocean circulation is also modulated by internal variability that cannot directly be attributed to the forcing by winds and air-sea fluxes. This internal ocean variability

OSD
9, 3191–3238, 2012

depends on the actual conditions (temperature, salinity, velocities) of the ocean at any given time rather than on the atmospheric conditions. A well known example of ocean variability that is in general not directly linked to atmospheric variability are mesoscale ocean eddies, which can be regarded as the ocean equivalent of weather systems in the atmosphere (Williams et al., 2007). As for high and low pressure systems in the atmosphere the time and location of formation of ocean eddies depends on initial conditions, i.e. in a numerical ocean model even a small perturbation in the initial ocean conditions (temperature, salinity, velocities) will eventually lead to a different mesoscale eddy field, in the same way as perturbed initial conditions in a weather forecasting model will typically lead to different weather patterns in a matter of days. As with weather systems, we cannot predict the mesoscale eddy field a long time in advance even if the areas where ocean eddies tend to develop (e.g. along the Antarctic Circumpolar Current, in the Agulhas retroflection region, extensions of Kuroshio and Gulf Stream) are well known. The longer life times and slower propagation of ocean eddies mean they can be predicted on longer timescales than their atmospheric counterparts. However, the ocean mesoscale eddy field generally becomes largely unpredictable on timescales of several months (Stammer, 1997). Mesoscale eddies may also interact with topography (e.g. when they approach a continental margin) which mean that they can trigger internal waves such as baroclinic Kelvin and Rossby waves. As a consequence the internal wave field will also be unpredictable to some extent. Note that the internal wave field is more predictable than eddies since, e.g., Rossby waves generated by up- and downwelling along coastlines can readily be linked to atmospheric wind forcing.

The understanding of the potential predictability of ocean currents is a subject of ongoing research and is growing in importance. Operational ocean forecasting systems (e.g. Drevillon et al., 2008; Martin et al., 2007) now routinely provide weekly forecasts of the ocean conditions based on eddy-permitting and increasingly on eddy-resolving models. However, most research to date into the predictability of ocean currents such as the meridional overturning circulation (MOC) is based on coarse resolution ocean

OSD
9, 3191–3238, 2012

models where mesoscale eddies are not resolved (Collins and Sinha, 2003; Hawkins and Sutton, 2009; Sévellec, 2008; Zanna and Tziperman, 2005). Ocean eddies are ubiquitous and therefore this raises the question how much they affect the variability of the ocean circulation not only in terms of temperatures, salinity, ocean colour... etc. but also how they impact the variability of components of the ocean circulation such as western boundary currents, or the MOC. The important role of eddies in the transport of heat, freshwater and in the mixing of water masses has been widely acknowledged (e.g. Jayne and Marotzke, 2001). However, how big an imprint ocean eddies may leave on the variability of the MOC is far from fully understood, but is crucial for the interpretation of observational MOC estimates. The MOC plays a key role in maintaining the current climate in the North Atlantic region and in recent years much effort has been dedicated to observing its strength and variability (Cunningham et al., 2007; Kanzow et al., 2009, 2010; Rayner et al., 2011). The variability inferred from such systems is affected by mesoscale ocean eddy activity but it is difficult to quantify the effect. Based on the amplitude of the observed sea surface height variability (SSH) Wunsch (2008) suggests that the eddy imprint on meridional transports could exceed 20 Sv ($1\,\mathrm{Sv} = 10^6\,\mathrm{m^3 s^{-1}}$). According to this study the MOC would therefore be potentially subject to a very large eddy related variability. This view was challenged in a study by (Kanzow et al., 2009) who show that the large sea surface height (SSH) variability which was projected onto meridional transports in (Wunsch, 2008) dramatically decreases close to the western margin. Furthermore, when moving closer to the western boundary the correlation between SSH and meridional transports gradually weakens, suggesting that SSH is not a good indicator for zonally integrated basin-wide transports. Therefore the projection of SSH anomalies onto the MOC is not straightforward (Kanzow et al., 2009; Hirschi et al., 2009). Nevertheless, the question of how large the imprint of unpredictable ocean processes on the MOC is, remains and in this study we use a global ocean model to investigate the forced and unpredictable or "chaotic" MOC components. The aim of the present paper is to provide an estimate of the dependence of the MOC on initial conditions across subannual to interannual timescales.

OSD
9, 3191–3238, 2012

In the remainder of this paper we will refer to the "initial condition dependent" MOC variability as the "chaotic" MOC variability. The model and method used in our study are presented in Sects. 2 and 3. Results showing the amplitude of the chaotic MOC variability are presented in Sect. 4. Our findings are discussed and summarised in Sects. 5 and 6.

2 Model description

The ocean model used in this study is the Nucleus for European Modelling of the Ocean (NEMO) in the ORCA025 and ORCA1 configurations (Madec, 2008). The ORCA025 configuration is similar to the one used in (Blaker et al., 2012). For both resolutions, the model has 64 vertical levels with layer thickness increasing from 6 m at the surface to more than 200 m at the bottom. The surface forcing consists of 6-hourly winds and daily fluxes for heat and freshwater from the DFS3 dataset (Brodeau et al., 2010). For salinity a weak restoring with a time constant of 180 days is used to prevent salinities from drifting.

With a horizontal resolution of 1/4° ORCA025 is eddy-permitting, i.e. ORCA025 can simulate ocean mesoscale eddies, but their dynamics is not resolved. Nevertheless, a horizontal resolution of 1/4° has been shown to produce satisfactory eddy activity even if the eddy kinetic energy is lower than suggested by satellite observations (e.g. Donners et al., 2004; Penduff et al., 2010). For ORCA1 the horizontal resolution is 1°, except between 19.6° N and 19.6° S where the meridional resolution is smoothly increased to about 1/3° at the Equator.

The results discussed in this paper are based on two twin experiments performed with ORCA025 and ORCA1. Each twin experiment consists of two passes through the surface forcing for the years 1958 to 2001. From here onwards the first passes in ORCA025 and ORCA1 will be referred to as experiments A025 and A100 respectively, while the second passes will be referred to as experiments B025 and B100. Both simulations A025 and A100 start from rest with initial conditions for temperatures and

OSD
9, 3191–3238, 2012

salinities taken from the World Ocean Atlas (Antonov et al., 1998). In experiments B025 and B100 the forcing for the 1958 to 2001 period is repeated but now the ocean initial conditions are taken from the end of experiments A025 and A100 (i.e. ocean state at the end of 31st December 2001).

Strong drifts are found in the ocean circulation during the first 10–15 years of A025 and A100. These drifts are visible in transports such as the Antarctic Circumpolar Current (ACC) and the MOC. After this initial phase the ocean transports reach a quasi steady state. Note that after this initial adjustment phase there is still a smaller long-term drift. For the MOC this long-term drift is typically about 2 Sv/century (compared with about 1 Sv/year at the beginning of A025 and A100). These long-term drifts reflect the long-term adjustment of the ocean to the surface forcing. For the deep ocean this adjustment can take hundreds or even thousands of years - much longer than we can afford to run with ORCA025.

In the remainder of this study we will avoid the initial adjustment phase with strong MOC drifts and we will only consider the last 25 years of A025, A100, B025, B100, i.e. the years 1976 to 2001. The MOC strength and structure is similar for both model resolutions used here and is illustrated for experiment B025 for the 1976 to 2001 period (Fig. 1). In the Atlantic the MOC consists of two overturning cells linked to the formation of North Atlantic Deep Water (NADW) and Antarctic Bottom Water (AABW). The NADW cell ranges from the surface to depths of about 3000 m. With values of about 16 Sv the maximum transport in the NADW cell occurs at 35° N at 1000 m depth. During the 1976 to 2001 period considered here the mean Atlantic MOC in NEMO is comparable to other similar models (e.g. Hirschi and Marotzke, 2007). At 26° N the MOC is around 16 Sv which is slightly weaker than the 18 Sv suggested by observations at that latitude (Cunningham et al., 2007; Kanzow et al., 2009; Rayner et al., 2011). The AABW cell fills the deep ocean below 3000 m and reaches maximum values of about 2 Sv. The Indo-Pacific is dominated by the AABW cell and apart from the uppermost layers which are dominated by Ekman transports the AABW cell reaches its maximum values of 6–8 Sv between 3000 and 4000 m depth. In the following sections we will show that a careful

OSD
9, 3191–3238, 2012

comparison of the MOC variability found in A025/A100 and B025/B100 can be used to estimate the amplitude of the chaotic MOC variability on subannual to interannual timescales.

3 Method

The twin experiments A025/A100 and B025/B100 will now be used to estimate to what extent the MOC variability on sub- to interannual timescales is either directly forced by the atmosphere (i.e. deterministic) or internally generated (i.e. chaotic). Since the prescribed atmospheric fields being fed into the bulk formula (Large and Yeager, 2004) are identical the surface forcing experienced by the ocean in the twin experiments is similar. We will show that differences between the twin experiments mainly arise from different initial conditions in the ocean.

Some of the differences between the model passes reflect the long-term model drift described in the previous section and the initial conditions for the second model passes (experiments B025 and B100) do contain the model drift that occurred during the first passes (experiments A025 and A100). The model drift is a gradual and monotonic process (i.e. small drifts in the order of 2 Sv/century for the MOC in B025) which leads to changes in the long term means of temperature, salinity, and currents. However, in addition to these long term changes which reflect a long-term imbalance between the surface forcing and the ocean state, there are also differences between A025 and B025 (and A100, B100) that occur on shorter timescales. These differences are not monotonic (i.e. no gradual drift towards warmer/colder conditions or stronger/weaker transports) but can be of either positive or negative sign. Such changes can be illustrated when comparing the sea surface height (SSH) in experiments A025 and B025. A large fraction of the SSH variability in A025 and B025 is due to mesoscale eddy activity (e.g. Penduff et al., 2011). The timing and location of eddies depend on initial conditions, i.e. if the same dates are considered in A025 and B025 the mesoscale eddy fields are largely uncorrelated. This is illustrated for the North Atlantic in Fig. 2 which

OSD
9, 3191–3238, 2012

shows the correlation between 5-day mean SSH values in A025 and B025 as well as between A100 and B100. Regions where eddy variability is high in A025 and B025 (e.g. the Gulf Stream and North Atlantic Current) are characterised by correlations that are close to zero. These low correlations are not due to a systematic change in the SSH (i.e. a long term model drift) but reflect SSH values fluctuating around similar mean values but with a timing that is different between experiments A025 and B025. Other regions where low correlations are found for the SSH between A025 and B025 are the Kuroshio and its eastward extension, the confluence of Brazil and Malvinas Currents, the Agulhas region, and the Southern Ocean (not shown). As we expect the absence of mesoscale ocean eddies leads to much higher correlations between the SSH variability in experiments A100 and B100. This indicates that the chaotic variability is smaller in the ORCA1 simulations, but this will be discussed in more detail later in the paper.

Differences between the model passes 1 and 2 are not confined to SSH (i.e. mainly to the ocean eddy field) but will also be seen in ocean transports such as the MOC. To illustrate how we will quantify the amplitude of the chaotic MOC variability on sub- to interannual timescales we introduce a conceptual model. The basic setup of this simple box-model (Fig. 3) consists of a Stommel-type two-box configuration (Stommel, 1961) which allows us to represent the exchange of water masses between high and low latitudes driven by a meridional density gradient. The governing equations for the box model are

$$\rho_1(t+\Delta t) = \frac{(\rho_1(t)\cdot(V_1 - q\Delta t) + q\Delta t\rho_2(t))}{V_1} \quad (1)$$

$$\rho_2(t+\Delta t) = \frac{(\rho_2(t)\cdot(V_2 - q\Delta t) + q\Delta t\rho_1(t))}{V_2} \quad (2)$$

$$q(t) = \beta(\rho_1(t) + \zeta_1(t) - \rho_2(t) - \zeta_2(t)) \quad (3)$$

$$F_1(t) = \alpha(\rho_1^* + \epsilon_1(t) - \rho_1(t)) \quad (4)$$

$$F_2(t) = \alpha(\rho_2^* + \epsilon_2(t) - \rho_2(t)) \quad (5)$$

OSD
9, 3191–3238, 2012

where q is the transport between the two boxes and β a constant scaling factor. F_1, F_2 are the air-sea fluxes where (non-dimensional) pseudo densities ρ_1, ρ_2 are restored against ρ_1^*, ρ_2^* with a time constant α. V_1, V_2 are the box volumes and ϵ_1, ϵ_2 and ζ_1, ζ_2 are "atmospheric" and "oceanic" noise, respectively.

The conceptual model allows us to produce analogues to the NEMO experiments with the main difference that here we can simply switch on/off the chaotic "ocean" variability $\zeta_{1,2}$. To estimate the amplitude of chaotic "ocean" variability in the transport q we can simply run the model with and without "ocean" noise (i.e. $\zeta_{1,2}(t) \neq 0$, $\zeta_{1,2}(t) = 0$). The "atmospheric" noise $\epsilon_{1,2}(t)$ is the same in both box-model runs. Apart from an initial spin-up phase, the difference between q in two such runs is then due to differences in the noise $\zeta_{1,2}(t)$ (i.e. the "chaotic ocean variability", Fig. 4). The amplitude of the "chaotic" variability in q can therefore be quantified by simply calculating the standard deviation of the difference.

We can also easily obtain a pair of box-model simulations equivalent to A025 and B025 by running the box-model with different realisations of the "ocean" noise $\zeta_{1,2}$ (temporally uncorrelated, but with the same amplitude) in both simulations, whereas the "atmospheric" variability $\epsilon_{1,2}$ is identical in both model passes. The timeseries of q are the box-model equivalents of MOC timeseries from A025 and B025. However, taking the difference between passes 1 and 2 leads to an overestimation of the amplitude of the chaotic variability (Fig. 4b). Since the "chaotic" ocean variability in both runs is uncorrelated (different white noise $\zeta_{1,2}$ in both runs) values larger than the extremes in $\zeta_{1,2}$ can occur for the difference between the two model passes. For both runs the chaotic ocean variability is white noise of the same amplitude. The timeseries of differences between q in passes 1 and 2 therefore has to be larger according to

$$\sigma(q_1 - q_2)^2 = \sigma(\Delta q_1)^2 + \sigma(\Delta q_2)^2 - 2 \cdot \mathrm{cov}(\Delta q_1, \Delta q_2), \quad (6)$$

where σ denotes the standard deviation, cov the covariance, $\Delta q_{1,2}$ the differences between q obtained with $\zeta_{1,2} = 0$ and q obtained with two different realisations of $\zeta_{1,2} \neq 0$. For uncorrelated timeseries (as is the case for two different white noise series) the standard deviation for the difference $q_1 - q_2$ exceeds the standard deviation of $\Delta q_{1,2}$ by

OSD
9, 3191–3238, 2012

a factor of $\sqrt{2}$, i.e. to obtain the correct estimate of the amplitude of the "chaotic" ocean variability $\sigma(q_1 - q_2)$ needs to be scaled by $1/\sqrt{2}$. Depending on the correlation of the "chaotic" ocean variability the scaling factor can change between 0 (perfect correlation of the noise between both model passes, and 2 (perfect anticorrelation, Fig. 5).

The simple box model shows that the difference between two NEMO simulations with the same atmospheric forcing but different chaotic ocean variability overestimates the amplitude of the chaotic ocean variability. The main driver of chaotic variability in NEMO is the presence of mesoscale eddies. As shown previously the correlations between the eddy fields in experiments A025 and B025 are low (Fig. 2) and for the remainder of this study we will assume that the imprint of eddies (and to a lesser extent also of internal waves) are decorrelated in experiments A025 and B025. As in the box-model we will use the standard deviation of the differences between A025 and B025 (and between A100 and B100) to provide a measure of the amplitude of the chaotic MOC variability.

Note that the method introduced above will allow us to provide a quantitative estimate of the chaotic MOC variability in a statistical sense. This means that we will only be able to make statements about the chaotic MOC variability on timescales that are short compared to the duration of the simulations. Since we want to avoid of the initial phase of the model integrations where strong drifts occur, we are limited to 25-year long datasets (period from 1976 to 2001). We can therefore obtain estimates of the standard deviation of the chaotic MOC variability on subannual to interannual timescales, but we will not be able to comment on the likely amplitude of the chaotic MOC variability on decadal timescales.

4 Results

The approach introduced in Sect. 3 is now applied to the years 1976 to 2001 of the NEMO experiments A025, B025, A100, and B100.

OSD
9, 3191–3238, 2012

4.1 MOC variability

The MOC variability in experiments A025 and B025 ranges from subdaily to interannual timescales (Blaker et al., 2012). The short duration of the simulation means that we cannot comment on decadal and longer timescales. Since we use 5-day averages we also cannot address to what extent the subdaily MOC variability generated by near inertial gravity waves (Blaker et al., 2012) is affected by chaotic processes. Based on 5-day averages the largest standard deviations for the MOC in the Atlantic are typically around 3–4 Sv in mid to high latitudes (Fig. 6a). A much larger variability characterises the Equatorial region where the standard deviation reaches up to 23 Sv. A similar variability pattern is found for the Indo-Pacific (Fig. 6b). The main difference is that the standard deviation is 2–3 times larger. At mid latitudes values are typically between 6–8 Sv, while values of up to 60 Sv are found at the Equator. The larger MOC variability in the Indo-Pacific is mainly due to the much wider basin which allows for higher values in Ekman transport and in its variability. An interesting feature is the very high variability found at the Equator. Whereas a maximum MOC variability at the Equator is expected (e.g. Jayne and Marotzke, 2001) the values found in NEMO are higher than those found in other models. There is only little dependence of the Equatorial variability on the model resolution. In experiments A100 and B100 the maximum standard deviation for the MOC at the Equator is 20 Sv in the Atlantic – only marginally smaller than the value found in experiments A025 and B025 (not shown). Trying to explain why NEMO produces a higher Equatorial variability than other ocean models is beyond the scope of this paper and is the subject of ongoing research. The only other model we are aware of that produces a similar variability is the model from the Los Alamos Parallel Ocean Program (POP) (Alicia Karspeck, personal communication).

In analogy to the simple box-model introduced earlier, the correlations between the model passes 1 and 2 are high (Fig. 7). This is illustrated for A025 and B025 at 26° N in the Atlantic and in the Indo-Pacific. In the Atlantic (Indo-Pacific) the MOC is slightly weaker (stronger) in B025 than in A025, but the timing of MOC peaks and troughs

OSD
9, 3191–3238, 2012

remains essentially the same in both model passes (Fig. 7a, b, d, e). However, the temporal agreement between both model passes is not perfect. The difference in transports between A025 and B025 is not just a constant offset or gradually increasing/decreasing (e.g. due to model drift) but it exhibits peaks and troughs with a typical duration of a few months (Fig. 7c, f). In both the Atlantic and Indo-Pacific the amplitude of the MOC difference between A025 and B025 exhibit peak-to-peak differences that can exceed 5 Sv. In accordance to the findings from the box model we have scaled the difference between the two model passes by $1/\sqrt{2}$. In the remainder of the paper we will look at the unfiltered values (i.e. 5-day averages) of MOC or of the difference between both model passes as well as at the subannual and interannual components of the variability. The interannual variability is obtained by smoothing the MOC with a Parzen filter and the subannual variability is then given by the difference between the unfiltered and the filtered timeseries (Fig. 7c, f).

Correlations between A025 and B025 for the MOC as a function of latitude and depth show that at most depths the correlations are 0.8 or higher in all the regions examined (Atlantic, Indo-Pacific and Southern Ocean, Figs. 8 and 9). In the surface layers correlations are higher than 0.9 at all latitudes on both sub- and interannual timescales. This is expected as the MOC in the surface layers is dominated by Ekman transports. Given that the same atmospheric forcing fields are passed to the bulk formula (Large and Yeager, 2004) in the twin experiments the surface wind stress experienced by the ocean in the twin simulations will be similar. Note that the wind stress is not exactly the same in the twin runs since it depends on the difference between the wind-speed and the ocean velocities. The ocean velocities for any given time and location will differ between the twin runs which leads to the ocean experiencing a different wind stress. However, our results show that the impact of different ocean velocities on the wind stress is small when we look at zonally integrated transports such as the MOC and that very similar Ekman transports occur in both A025 and B025. The lowest correlations of 0.6 or less are found in the bottom layers. However, at these depths the MOC variability is weak (Fig. 6). Correlations between A025 and B025 are higher in the Indo-Pacific than in the

OSD
9, 3191–3238, 2012

Atlantic. As before this can be explained by the dominance of Ekman variability in the Pacific MOC. Since the wind fields prescribed in A025 and B025 are identical the resulting wind stresses will be very similar. The same holds true for the Atlantic but firstly, the Atlantic is narrower, which means weaker Ekman transports and variability, and secondly, the Atlantic is characterised by the clockwise overturning cell linked to deep water formation in the Nordic Seas (Fig. 1). The total variability of the Atlantic overturning cell contains a large contribution from geostrophic transports (Hirschi et al., 2007; Cunningham et al., 2007). In the Indo-Pacific this contribution is much smaller.

It is also interesting to note that correlations are very high (>0.9) at the Equator in both the Atlantic and the Indo-Pacific. This suggests that the large Equatorial variability described earlier can largely be predicted from the surface forcing. The lowest correlations are found South of 30° S in the Atlantic and at the latitudes of the Antarctic Circumpolar Current (ACC acronym already introduced) for the global MOC (Fig. 9). However, even for these locations the correlations are higher than 0.7 at the depths where the maximum MOC occurs. A reduced correlation in the South Atlantic can be expected as this region is affected by Agulhas rings that are shed at the southern tip of Africa and which have been shown to affect the MOC variability (Biastoch et al., 2008). As with other ocean eddies the timing of the formation of Agulhas rings depends more on the ocean conditions than on the surface forcing at the time when the ring forms. In summary, the high correlations between the two model passes A025 and B025 shown in Figs. 8 and 9 suggest that on subannual to interannual timescales the MOC variability can be largely predicted from the surface forcing.

In the top 1000 m the correlation values between the MOC in A025 and B025 are similarly high (0.8 to 0.9) on subannual and interannual timescales. At depths below 1000 m the correlation is lower on interannual than on subannual timescales. This is most pronounced in the Atlantic where we find correlations of 0.1 or less in the deepest layers (Fig. 8c). In the Indo-Pacific the correlation generally remains above 0.6 even at great depths on both sub- and interannual timescales (Fig. 8e, f).

OSD
9, 3191–3238, 2012

4.2 Chaotic MOC variability

The correlation between the MOC in A025 and B025 is high. Nevertheless, looking at the difference between the model passes shows that there is a non-negligible fraction of the MOC variability that cannot directly be linked to the surface forcing. In analogy to the box-model we calculate the amplitude of the chaotic MOC variability according to

$$\Psi_{\mathrm{cha}}(y,z,t) = (\Psi(y,z,t)_{A025} - \Psi(y,z,t)_{B025})/\sqrt{(2)}, \quad (7)$$

where $\Psi(y,z)_{A025}$ and $\Psi(y,z)_{B025}$ are the meridional streamfunctions for the model passes A025 and B025. As for the correlations we just discussed we look at the total, subannual and interannual chaotic MOC variability (Fig. 10). In the Atlantic (Fig. 10a, b, c) the standard deviation of the chaotic MOC variability Ψ_{cha} reaches more than 3 Sv at the Equator at a depth of 3000 m. Away from the Equator the maximum variability is typically between 0.8 and 1.5 Sv and occurs at depths between 1000 and 3000 m. The chaotic MOC variability is larger in the South Atlantic with values of up to 2 Sv at the southern limit of the domain. Looking at the subannual variability reveals that most of the chaotic MOC variability occurs on short timescales. The values for the standard deviation of the subannual chaotic MOC variability are only slightly reduced compared with the values found for the total chaotic MOC. On interannual timescales the chaotic MOC variability is much smaller with values of less than 0.5 Sv over most of the Atlantic domain.

For the Indo-Pacific (Fig. 10d, e, f) we also find a pronounced variability maximum in Ψ_{cha} at the Equator with a standard deviation of up to 7 Sv (Fig. 10d, e). As in the Atlantic this Equatorial variability occurs on subannual timescales. Apart from a band of latitudes between 15° S and 15° N the standard deviation of the subannual variability in Ψ_{cha} is between 1 and 1.5 Sv – values which are similar to the chaotic variability found in the Atlantic. On interannual timescales the chaotic MOC variability in the Indo-Pacific is 0.5 Sv or less at most latitudes. Again this is comparable with the Atlantic values.

OSD
9, 3191–3238, 2012

The ratio of the chaotic to the total MOC variability can be given as the ratio Ψ_{cha}/Ψ (Fig. 11). The lowest ratios are found in the top few hundred metres. This is expected as a large fraction of the MOC variability in the top layers is due to variability in the Ekman transports which only differ slightly between the two model passes. The ratio gradually increases with depth and at 1000 m, which is approximately where the MOC typically reaches its maximum, values are mostly between 0.2 to 0.3. It is noteworthy that even though the largest MOC variability is found at the Equator, this region coincides with low ratios (<0.2) between chaotic and total MOC variability. This low ratio is consistent with the high correlations found at the Equator (Fig. 8) and confirms that the large Equatorial MOC variability in NEMO is highly predictable from the surface forcing.

The highest ratios mostly occur at the bottom with values that can be in excess of 1. However, at great depths the MOC variability is small compared to the values found around the depths where the maximum MOC occurs (Fig. 6). Between depths of 1000 and 3000 m, the highest ratios in the Atlantic are found south of 20° S with values between 0.3 and 0.5 (Fig. 11a). This is higher than the corresponding ratios found in the North Atlantic. The increased fraction of chaotic MOC variability in the South Atlantic is likely to be linked to strong eddy activity at the southern limit of the region as will be discussed in more detail in Sect. 5. An interesting feature is that the ratio between the chaotic and total MOC variability increases when moving from subannual to interannual timescales (Fig. 11b, c). This is most pronounced south of 25° N and at depths greater than a few hundred metres. At depths of around 2500 m where the maximum interannual MOC variability occurs the ratio can reach values in excess of 0.6, suggesting that a substantial fraction of the interannual MOC variability is of chaotic nature. North of about 30° N the ratio between chaotic and total MOC variability are comparable for subannual and interannual timescales. However, as shown in Fig. 10, the chaotic MOC variability is small on interannual timescales.

In the Indo-Pacific ocean the ratio between chaotic and total MOC variability is lower than in the Atlantic (Fig. 11d, e, f). This is expected since the amplitude of the chaotic MOC variability is similar in both the Atlantic and the Indo-Pacific whereas the total

OSD
9, 3191–3238, 2012

MOC variability is higher in the Indo-Pacific than in the Atlantic (Fig. 6). As in the Atlantic low ratios are found at the Equator. This means that in the Indo-Pacific the large Equatorial variability is also largely predictable from the surface forcing. Again this is consistent with the high correlations been the two model passes in the Indo-Pacific (Fig. 8).

The Antarctic Circumpolar region is a region of high eddy activity and Fig. 12a shows that this region coincides with the largest chaotic MOC variability away from the Equator. Between 40° S and 60° S the standard deviation of the total chaotic MOC variability can reach up to 3 Sv. Compared with the total MOC variability for the Southern Ocean this leads to ratios of 0.4 to 0.6 (Fig. 12b) which are similar to the ones shown earlier for the South Atlantic (Fig. 10). As for the Indo-Pacific and Atlantic most of the chaotic MOC variability occurs on subannual timescales with much less variability found on interannual timescales (not shown).

An underlying assumption of this study is that the amplitude of the chaotic MOC variability depends on the presence or absence of mesoscale ocean eddies. It is therefore worthwhile knowing to what extent the MOC variability found in the non eddy-permitting experiments A100 and B100 is chaotic. For both the Atlantic and the Indo-Pacific the ratio between the chaotic and the total MOC variability is 0.1 or less for most latitudes and depths (Fig. 13a, b, d, e). This is much less than the fractions found for the eddy-permitting experiments A025 and B025. On interannual timescales the chaotic MOC variability accounts for fractions that are comparable to those seen for experiments A025 and B025. However, these high ratios are mostly found below 1000 m depth i.e. below the depth where the largest MOC values tend to occur (Fig. 13c, f).

In order to get more insight into the nature of the chaotic MOC variability it is useful to look at Hovmöller diagrams of the MOC differences between experiments A025 and B025 (Fig. 14). On both subannual and interannual timescales the chaotic MOC variability exhibits meridional bands of coherence. In the Atlantic the largest subannual coherent features occur in the South Atlantic (Fig. 14a). The latitude band between 35° S and the Equator is characterised by coherent bands with alternative positive and

OSD
9, 3191–3238, 2012

negative values for the chaotic MOC variability. Such a large meridional coherence is not found in the North Atlantic which instead is characterised by three bands of coherence: between the Equator and about 10° N, from 10° N to 25° N, and from 25° N to about 35° N. North of 35° N there is an indication of northward propagating features. Hints of a northward propagation in the North Atlantic are found between the two northernmost bands of coherence most likely reflecting anomalies propagating along the North Atlantic Current. The different bands of coherence in the North Atlantic are likely to reflect the more fractured coastlines compared to the South Atlantic. Perturbations mediated through waves trapped along the continental margins have to follow longer, more tortuous pathways to propagate meridionally in the North Atlantic which would explain the less coherent picture seen for the chaotic MOC fluctuations in the North Atlantic than in the South Atlantic.

On interannual timescales the values for the chaotic MOC variability are between –1.5 and 1.5 Sv (Fig. 14b). The Equatorial "barrier" that characterised the subannual timescales appears much reduced and there are several instances of MOC fluctuations crossing the Equator. In the northern hemisphere there is still some indication of the three meridional bands of coherence (10° N, 25° N and 40° N) found for the subannual chaotic MOC variability. The amplitude and meridional extent of the interannual signals are similar to the MOC variability signals described by (Biastoch et al., 2008) where the authors investigate the impact of mesoscale eddies in the Agulhas region on the variability of the Atlantic MOC. A feature common to both subannual and interannual timescales is the clear northern limit at about 40° N. Beyond this latitude the amplitude of the chaotic MOC variability is much reduced and meridionally coherent features are no longer seen. This contrasts with the meridional coherence found when looking at anomalies of the MOC in experiment B025 after removing the Ekman contribution (Fig. 15). Here latitudinally coherent MOC bands are not confined south of 40° N but also characterise a latitude band between 40° N and 60° N. This is similar to the results documented by Bingham et al., 2007 for a coupled (HadCM3) and an ocean-only model

OSD
9, 3191–3238, 2012

(OCCAM). South of 40° N the MOC anomalies in B025 exhibit different coherent bands with meridional extents similar to those seen for the chaotic MOC.

The meridional coherence of the chaotic MOC variability in the Indo-Pacific is comparable to its Atlantic counterpart with coherent MOC bands characterising the latitudes south of about 40° N (Fig. 14c, d). The largest chaotic variability at 1000 m depth occurs at the Equator and around 10° S, coinciding with the Indonesian Throughflow. Maximum chaotic variability around 10° S is found on subannual and interannual timescales and the amplitude of the chaotic MOC fluctuations can exceed 5 Sv (Fig. 14c, d). These fluctuations are likely linked to the variability of the Indonesian Throughflow which contains a large chaotic (unforced) variability. However, as is indicated by the high correlations between the model passes 1 and 2 (Fig. 8) as well as the low ratios in Fig. 11, the chaotic variability around 10° S is small compared to the total MOC variability.

Away from the latitudes affected by the Indonesian Throughflow, the peak-to-peak values of the chaotic MOC variability and its meridional coherence are similar to what we find in the Atlantic. Values are typically a few Sv which is consistent with the amplitudes found for the standard deviations of the chaotic MOC variability in the Indo-Pacific and Atlantic described earlier in this section (Fig. 10). As in the Atlantic, 40° N appears to be a barrier to the chaotic MOC signals in the Indo-Pacific and little chaotic MOC activity occurs further North. As before this is different from the behaviour found for the full MOC (with Ekman component removed) which shows a meridionally coherent variability between 40° N and 60° N (Fig. 15c, d).

5 Discussion

The main motivation for this study is to gain a better understanding of the impact that chaotic ocean processes, in particular mesoscale ocean eddies could have on observations of the MOC. Recent observational programmes have dedicated much effort to observing the MOC. The results have shown that the MOC can exhibit large variability on short (subannual) timescales – a variability that is only partly understood. The

OSD
9, 3191–3238, 2012

question of how much of the observed signal reflects eddy (and internal wave) activity cannot be addressed directly from the existing observations. A study by (Wunsch, 2008) suggested a possible eddy imprint that could exceed the full MOC signal observed at 26.5° N. A thorough study by (Kanzow et al., 2009) demonstrated that the imprint of eddies on the MOC is much smaller. However, the observational data currently available do not allow a quantification of the chaotic MOC variability.

Our results suggest that the chaotic MOC variability accounts for a few Sv of the total MOC variability. When the depth of the maximum MOC is considered (typically at about 1000 m depth), about 20 to 30 % (Atlantic), respectively 10 % (Indo-Pacific) of the MOC variability is chaotic. Conversely, this also means that 70 to 80 % (Atlantic), respectively 90 % (Indo-Pacific) of the MOC variability can directly be attributed to the surface forcing (winds, heat and fresh water fluxes). The fact that on sub- to interannual timescales the MOC variability mainly reflects the surface forcing is illustrated by the high correlations (Fig. 8) between the numerical experiments A025 and B025 (A100, B100). The main implication is that on sub- to interannual timescales the MOC variability is largely predictable from the surface forcing conditions. Despite being of a sizeable amplitude the chaotic (non-deterministic) MOC variability is too small to affect the overall MOC variability. This also means that the variability of the MOC that has been observed since 2004 at 26.5° N in the North Atlantic is unlikely to mainly reflect processes such as mesoscale ocean eddies or internal waves that are not directly linked to the surface forcing. At the same time the high correlations between the model passes 1 and 2 also suggest that a good knowledge of the surface forcing might be enough to estimate the MOC not just at the surface but even down to greater depths. To obtain the correlation patterns shown in Fig. 8 one does not need the full 25 years (1976 to 2001) of model data but the correlation patterns look almost identical if only half the data were used (e.g. 1976 to 1988, not shown). This means that one could just build a simple linear regression model based on the relationship between the surface forcing and the MOC relationship for the years 1976 to 1988 that can then be used to predict the MOC for the years 1989 to 2001 from the surface forcing alone. Our results suggest that such

OSD
9, 3191–3238, 2012

a simple model would do a good job not just for the obvious Ekman component in the surface layers but also down to depths of at least 1000 m which typically coincide with the depth at which the MOC reaches its maximum value. Of course based on our results we can only comment on sub- to interannual timescales. To assess whether the relationship between the variability in the surface forcing and the MOC also holds on decadal and longer timescales would require longer simulations and cannot be answered in this study. It is also clear that a regression model as described above would not be capable of detecting a regime change (e.g. when fresh water forcing exceeds a critical threshold, leading to a major reorganisation of the MOC).

Despite the high correlations between the forcing and the MOC our results also show regions where the chaotic variability is a sizeable component of the total MOC variability. This is most pronounced in the South Atlantic. On interannual and to a lesser extent also on subannual timescales there is a gradual decrease of the correlations between passes 1 and 2 when moving towards the southern limit of the Atlantic domain. This is most pronounced below 2000 m depth. Whereas low correlations (and high ratios between chaotic and total MOC variability) are typically found in the bottom layers (where MOC values and variability are low) the South Atlantic is characterised by lower correlations at depths between 2000 and 3000 m depth where there is still a substantial MOC variability (Figs. 6 and 8). On interannual timescales the correlation between the surface forcing and the MOC is less than 0.7 over a large part of the water column in the South Atlantic, i.e. more than 50 % of the interannual variability cannot be explained by the surface forcing. This means that a substantial fraction of the variability of the (southward) meridional transports compensating the surface MOC branch is affected by internal processes such as mesoscale eddies and internal waves. So why is it that the chaotic MOC variability is more pronounced in the South Atlantic than in the North Atlantic? As mentioned earlier the largest differences between the two model passes occur because of a decorrelation of the mesoscale ocean eddy field (Fig. 2). However, why would mesoscale eddies have a larger imprint on the MOC in the South Atlantic than in the North Atlantic? Mesoscale ocean eddies are formed in both hemispheres

OSD
9, 3191–3238, 2012

with the Gulf Stream region as well as the southern tip of Africa or the area of the Zapiola anticyclone all showing lively eddy activity. A plausible reason why the imprint of chaotic processes in NEMO is larger in the South Atlantic than in the North Atlantic could be linked to the different depths down to which pronounced mesoscale activity occurs in our simulations (Fig. 16). When the surface layers are considered, both the North and South Atlantic seem to have similar mesoscale activities. However, this picture changes when moving deeper into the water column. Below depths of a few hundred metres the mesoscale activity is larger in the South Atlantic. From about 1000 m onwards there is only little mesoscale activity in the North Atlantic whereas the South Atlantic regions show mesoscale features down to depths of several thousand metres (Fig. 16). Note that qualitatively, it makes no difference whether the meridional velocities in Fig. 16 are plotted from either experiment A025, B025 or from their difference. The low correlations between mesoscale features in both model passes means that the inferred regions of high mesoscale variability are always same. An interesting feature is that the eddy variability found at greater depths in the Zapiola region extends almost to the continental margin therefore increasing the potential of these mesoscale features to directly affect the basin-wide density gradient and therefore basin-wide meridional transports (Hirschi and Marotzke, 2007; Hirschi et al., 2003).

What also emerges from Fig. 16 is that in the South Atlantic the regions of highest ocean eddy activity are found south of the southern limit where the Atlantic MOC can be computed (i.e. the southern tip of Africa). This means that signals have to propagate northward from the regions of high mesoscale activity. This is most likely to happen as boundary trapped Kelvin like waves along the east coast of South America. Such waves have been shown to rapidly transfer perturbations from high to low latitudes (e.g. Kawase, 1987; Hirschi and Stocker, 2002; ; Roussenov et al., 2008; Blaker et al., 2006) and it has been suggested that ocean mesoscale eddies can trigger boundary trapped waves (Kanzow et al., 2009). Looking at the chaotic MOC signals in the Atlantic at a high temporal resolution reveals that indeed the chaotic MOC fluctuations are propagating meridionally (Fig. 17) . The coherent MOC features between about 35° S and

OSD
9, 3191–3238, 2012

the Equator propagate from the southern limit of the Atlantic domain to the Equator in about one month. This corresponds to a propagation speed of slightly more than $1\,m\,s^{-1}$ which is close to the phase speed expected for baroclinic Kelvin waves. Compared to most other east coasts on the globe the South Atlantic east coast is smooth with an almost North-South orientation. This allows a fast meridional propagation of perturbations.

Further insight into the nature of the chaotic MOC variability could be gained by decomposing the MOC into its constituents (Ekman, thermal wind (i.e. geostrophic), and barotropic components e.g. Lee and Marotzke, 1998; Hirschi and Marotzke, 2007; Blaker et al., 2012). The correlations between the MOC in experiments A025 and B025 show that correlations are very high (>0.9) for all latitudes in the Atlantic and the Indo-Pacific in the surface layers (Figs. 8 and 9). This is a strong indication that Ekman transports are almost identical in the two model passes. Therefore, differences in the MOC in the twin simulations must have their origin in the thermal wind and barotropic components. However, the main goal of this paper is to provide an estimate of the amplitude the chaotic MOC variability and to describe its dependence on latitude, depth, and ocean basin. An analysis of the different MOC components is therefore beyond the scope of this paper and is left for a future study.

Another interesting and perhaps counterintuitive result of our analysis is that the chaotic MOC variability is not confined to timescales that are associated with the lifetime of mesoscale ocean eddies. On the contrary, the fraction of the chaotic MOC variability is higher on interannual than on subannual timescales (Fig. 11). Our results also show that at 1000 m where the maximum MOC tends to occur, the fraction of interannual MOC variability is larger in the eddy-permitting than in the non-eddying model (Figs. 11 and 13) therefore suggesting that the presence of ocean mesoscale eddies affects the chaotic MOC variability on interannual timescales. Studies have shown that the energy from mesoscale eddies does cascade to larger length scales (as well as the large scale flow can affect the eddy field, i.e. forward and backward energy cascades, e.g. Scott and Wang, 2005; Scott and Arbic, 2007). The presence of a chaotic MOC

OSD
9, 3191–3238, 2012

variability on longer timescales is also consistent with the results of a recent numerical study where the authors investigated the variability of sea surface height (SSH) in two NEMO 1/4° simulations forced with either climatological or interannual forcing (Penduff et al., 2011). Despite the absence of interannual forcing in the climatological simulation, the authors found that the amplitude of interannual SSH variability in the climatological simulation was between 40 and 80 % of the SSH variability found for the simulation using interannual atmospheric forcing. This suggests that even on interannual timescales a large fraction of the intrinsic SSH variability is not directly forced by the atmosphere but results from chaotic (intrinsic) ocean variability.

The estimates of the chaotic MOC variability obtained in this study have to be regarded as a lower limit. The eddying model that we use is eddy-permitting but not eddy-resolving. Therefore, the impact of eddies on the ocean variability is likely to be underestimated. Preliminary tests performed with a 1/12° version of NEMO suggest that the total MOC variability is about 20 % higher than in the 1/4° version used here, hinting to the possibility of a larger eddy-imprint on the MOC. Our results also only provide an indication of the amplitude of the chaotic MOC variability originating in the ocean provided that the atmospheric forcing is known. In the real world (as well as in coupled models where the ocean is eddying e.g. CM2.5/2.6, HadGEM3-H (Hewitt et al., 2010; Delworth et al., 2012) mesoscale ocean eddies can feed back onto the atmosphere. Therefore two coupled model simulations starting from identical atmospheric conditions as well as (apart from the ocean eddy field) from the same ocean will eventually experience different atmospheric conditions due to the different eddy-fields. After a certain number of months/years one model run may find itself in a prolonged positive NAO phase, whereas for the same dates the other simulation is in a negative NAO state. Such differences in the atmospheric conditions would obviously feed back onto the ocean and as a consequence the chaotic MOC variability of a coupled ocean-atmosphere system will be larger than the numbers reported in this study. The presence of mesoscale ocean eddies adds variability to the climate system with possible consequences for its predictability. More work is still required to gain a

OSD
9, 3191–3238, 2012

better understanding of possible impacts of mesoscale ocean eddies on climate variability/predictability if we want to make best use of the latest generation of coupled climate model using eddy-permitting (and soon eddy-resolving) ocean components that are currently being developed by research centres around the world.

6 Conclusions

We have studied the chaotic and forced MOC variability by comparing eddy-permitting and non eddy-permitting twin experiments which start from different initial conditions but which are forced with the same atmospheric forcing. We have found that:

- The MOC variability in the twin experiments is highly correlated on sub- to interannual timescales. High correlations are not confined to the obvious Ekman layer at the surface but reach down to several km. To a large extent the MOC directly reflects the atmospheric forcing on sub- to interannual timescales.
- In the presence of mesoscale ocean eddies the chaotic Atlantic MOC variability accounts for 20 % to 30 % (Atlantic) and 10 % to 20 % (Indo-Pacific) of the total MOC where the maximum MOC occurs (typically at a depth of around 1000 m). In the non-eddying case the chaotic MOC variability generally accounts for less than 10 % of the total MOC variability.
- The largest chaotic MOC variability occurs at the Equator with a standard deviation of 3 Sv (Atlantic) and 8 Sv (Indo-Pacific). However, this is only a small fraction (<10 %) of the very large Equatorial MOC variability (standard deviations of 23 Sv and 60 Sv in the Atlantic and Indo-Pacific, respectively). Away from the Equator the chaotic MOC variability is typically between 0.8 and 1.5 Sv and is similar in both Atlantic and Indo-Pacific
- The chaotic MOC variability exhibits meridional coherence. This is most pronounced in the South Atlantic where chaotic MOC anomalies are often coherent

OSD
9, 3191–3238, 2012

from about 35° S to the Equator. From the eddy rich region in the South Atlantic chaotic MOC anomalies propagate equatorwards with a speed comparable to that expected for a baroclinic Kelvin wave.

– Our results support earlier findings that the MOC observations at 26.5° N are unlikely to be strongly affected by eddy-induced variability. However, our estimate of chaotic MOC variability has to be regarded as a lower limit given that the model we used is eddy-permitting and not eddy-resolving.

Acknowledgements. This work was supported by the RAPID-WATCH project VALOR (NE/G007772/1) and was also part of the DRAKKAR project. We enjoyed discussions with Thierry Penduff and Florian Sévellec.

References

Antonov, J., Levitus, S., Boyer, T. P., Conkright, M., O'Brien, T., and Stephens, C.: Temperature of the Atlantic/Pacific/Indian Ocean, Vols 1-3, World Ocean Atlas 1998, Technical report, NOAA Atlas NESDIS 27, 166 pp., 1998. 3198

Biastoch, A., Böning, C. W., and Lutjeharms, J. R. E.: Agulhas leakage dynamics affects decadal variability in Atlantic overturning circulation, Nature, 456, 489–492, 2008. 3205, 3209

Bingham, R. J., Hughes, C. W., Roussenov, V., and Williams, R. G.: Meridional coherence of the North Atlantic meridional overturning circulation, Geophys. Res. Let., 34, L23606, 1–6, 2007. 3209

Blaker, A. T., Hirschi, J. J.-M., Sinha, B., de Cuevas, B., Alderson, S., Coward, A., and Madec, G.: Large near-inertial oscillations of the Atlantic meridional overturning circulation, Ocean Model., 42, 50–56, 2012. 3197, 3203, 3214

Blaker, A. T., Sinha, B., Ivchenko, V. O., Wells, N. C., and Zalesny, V. B.: Identifying the roles of the ocean atmosphere in creating a rapid equatorial response to a Southern Ocean anomaly, Geophys. Res. Lett., 33, L06720, doi:10.1029/2005GL025474, 2006. 3213

Bradley, R. S.: Quaternary Paleoclimatology: Methods od Paleoclimatic Reconstruction, Allen and Unwin, Boston, 1985. 3193

OSD

9, 3191–3238, 2012

Brodeau, L., Barnier, B., Penduff, T., Treguier, A.-M., and Gulev, S.: An ERA 40 based atmospheric forcing for global ocean circulation models, Ocean Modell., 31, 88–104, 2010. 3197
Collins, M. and Sinha, B.: Predictability of decadal variations in the thermohaline circulation and climate, Geophys. Res. Lett., 30, 391–394, doi:10.1029/2002GL016504, 2003. 3196
Cunningham, S. A., Kanzow, T., Rayner, D., Baringer, M. O., Johns, W. E., Marotzke, J., Longworth, H. R., Grant, E. M., Hirschi, J. J.-M., Beal, L. M., Meinen, C. S., and Bryden, H. L.: Temporal variability of the Atlantic Meridional Overturning Circulation at 26°N., Science, 317, 935–938, doi:10.1126/science.1141304, 2007. 3196, 3198, 3205
Czaja, A. and Frankignoul, C.: Observed Impact of Atlantic SST Anomalies on the North Atlantic Oscillation, J. Climate, 15, 606–623, 2002. 3194
Delworth, T. L., Rosati, A., Anderson, W., Adcroft, A. J., Balaji, V., Benson, R., Dixon, K., Griffies, S. M., Lee, H.-C., Paconowski, R. C., Vecchi, G. A., Wittenberg, A. T., Zeng, F., and Zhang, R.: Simulated climate change in the GFDL CM2.5 high-resolution coupled climate model, J. Climate, 25, 2755–2781, 2012. 3215
Donners, J., Drijfhout, S. S., and Coward, A. C.: Impact of cooling on the water mass exchange of the Agulhas rings in a high resolution ocean model, Geophys. Res. Lett., 31, doi:10.1029/2004GL020644, 2004. 3197
Drevillon, M., Bourdalle-Badie, R., Derval, C., Drillet, Y., Lellouche, J.-M., Remy, E., Tranchant, B., Benkiran, M., Greiner, E., Guinehut, S., Verbrugge, N., Garric, G., Testut, C.-E., Laborie, M., Nouel, L., Bahurel, P., Bricaud, C., Crosnier, L., Dombrowsky, E., Durand, E., Ferry, N., Hernandez, F., Galloudec, O. L., Messal, F.,and Parent, L.: The godae/mercator-ocean global ocean forecasting system: results, applications and prospects, J. Operat. Oceanogr., 1, 51–57, 2008. 3195
Hawkins, E. and Sutton, R.: Decadal Predictability of the Atlantic Ocean in a Coupled GCM: Forecast Skill and Optimal Perturbations Using Linear Inverse Modelling, J. Climate, 22, 3960–3978, 2009. 3196
Hewitt, T., Copsey, D., Culverwell, I. D., Harris, C. M., Hill, R. S. R., Keen, B., McLaren, A. J., and Hunke, E. C.: Design and implementation of the infrastructure of HadGEM3: the next-generation Met Office climate modelling system, Geosci. Model Develop. Discuss., 3, 1861–1937, doi:10.5194/gmdd-3-1861-2010, 2010. 3215
Hirschi, J., Baehr, J., Marotzke, J., Stark, J., Cunningham, S., and Beismann, J.-O.: A monitoring design for the Atlantic meridional overturning, Geophys. Res. Lett., 30, 1413–1416, 2003. 3213

OSD
9, 3191–3238, 2012

Hirschi, J. and Marotzke, J.: Reconstructing the meridional overturning circulation from boundary densities and the zonal wind stress, J. Phys. Oceanogr., 37, 743–763, 2007. 3198, 3213, 3214

Hirschi, J. and Stocker, T. F.: Rapid changes of the oceanic circulation in a hierarchy of ocean models, Tellus, 54A, 273–287, 2002. 3213

Hirschi, J. J.-M., Killworth, P. D., and Blundell, J. R.: Subannual, seasonal and interannual variability of the North Atlantic meridional overturning circulation, J. Phys. Oceanogr., 37, 1246–1265, 2007. 3205

Hirschi, J. J.-M., Killworth, P. D., and Blundell, J. R.: Sea surface height signals as indicators for oceanic meridional mass transports, J. Phys. Oceanogr., 39, 581–601, doi:10.1175/2008JPO3923.1, 2009. 3196

Imbrie, J., Boyle, E. A., Clemens, S. C., Duffy, A., Howard, W. R., Kukla, G., Kutzbach, J., Martinson, D. G., McIntyre, A., Mix, A. C., Molfino, B., Morley, J. J., Peterson, L. C., Pisias, N. G., Prell, W. L., Raymo, M. E., Shackleton, N. J., and Toggweiler, J. R.: On the structure and origin of major glaciation cycles, 1. linear responses to Milankovitch forcing, Paleoceanogr., 7, 701–738, 1992. 3193

Jayne, S. R. and Marotzke, J.: The Dynamics of Ocean Heat Transport Variability, Rev. Geophys., 39, 385–411, 2001. 3196, 3203

Johnson, H. L. and Marshall, D. P.: A theory of the surface Atlantic response to thermohaline variability, J. Phys. Oceanogr., 13, 1121–1132, 2002. 3213

Kanzow, T., Cunningham, S. A., Johns, W. E., Hirschi, J. J.-M., Marotzke, J., Baringer, M. O., Meinen, C., Chidichimo, M.-P., Atkinson, C., Beal, L. M., Bryden, H. L., and Collins, J.: On the seasonal variability of the Atlantic meridional overturning circulation at 26.5° N, J. Climate, 317, 938–941, 2010. 3196

Kanzow, T., Johnson, H. L., Marshall, D., Cunningham, S. A., Hirschi, J. J.-M., Mujahid, A., Bryden, H. L., and Johns, W. E.: Basin-wide integrated volume transports in an eddy-filled ocean, J. Phys. Oceanogr., 39, 3091–3110, 2009. 3196, 3198, 3211, 3213

Kawase, M.: Establishment of deep ocean circulation driven by deep water production, J. Phys. Oceanogr., 17, 2294–2317, 1987. 3213

Large, W. and Yeager, S.: Diurnal to decadal global forcing for ocean and sea-ice models: the data sets and flux climatologies, Technical report, CGD Division of the National Centre for Atmospheric Research, 2004. 3199, 3204

OSD

9, 3191–3238, 2012

Lee, T. and Marotzke, J.: Seasonal Cycles of Meridional Overturning and Heat Transport of the Indian Ocean, J. Phys. Oceanogr., 28, 923–943, 1998. 3214
Madec, G.: Nemo ocean engine, Technical report, Institut Pierre-Simon Laplace (IPSL), France, (Note du Pole de Modélisation, 27), 300 pp., 2008. 3197
Martin, M. J., Hines, A., and Bell, M. J.: Data assimilation in the FOAM operational short-range ocean forecasting system: a description of the scheme and its impact, Quart. J. Roy. Met. Soc., 133, 981–995, 2007. 3195
McPhaden, M. J.: Genesis and Evolution of the 1997-1998 El Niño, Science, 283, 950–954, doi:10.1126/science.283.5404.950, 1999. 3194
Penduff, T., Juza, M., Brodeau, L., Smith, G. C., Barnier, B., Molines, J.-M., Treguier, A.-M., and Madec, G.: Impact of global ocean model resolution on sea-level variability with emphasis on interannual time scales, Ocean Sci., 6, 269–284, doi:10.5194/os-6-269-2010, 2010. 3197
Penduff, T., Juza, M., Dewar, W. K., Barnier, B., Zika, J., Treguier, A.-M., Molines, J.-M., and Audiffren, N.: Sea-level expression of intrinsic and forced ocean variabilities at interannual timescales, J. Climate, 24, 5652–5670, 2011. 3199, 3215
Rayner, D., Hirschi, J. J.-M., Kanzow, T., Johns, W. E., Wright, P. G., Frajka-Williams, E., Bryden, H. L., Meinen, C. S., Baringer, M. O., Marotzke, J., Beal, L. M., and Cunningham, S. A.: Monitoring the Atlantic Meridional Overturning Circulation, Deep Sea Res., 58, 1744–1753, 2011. 3196, 3198
Roussenov, V. M., Williams, R. G., Hughes, C. W., and Bingham, R.: Boundary wave communication of bottom pressure and overturning changes for the North Atlantic, J. Geophys. Res., 113, C08042, doi:10.1029/2007JC004501, 2008. 3213
Scott, R. and Arbic, B.: Spectral Energy Fluxes in Geostrophic Turbulence: Implications for Ocean Energetics, J. Phys. Oceanogr., 37, 673–688, 2007. 3214
Scott, R. and Wang, F.: Dierct Evidence of an Oceanic Inverse Kinetic Energy Cascade from Satellite Altimetry, J. Phys. Oceanogr., 35, 1650–1666, 2005. 3214
Sévellec, F., Huck, T., Ben Jelloul, M., and Grima, N.: Optimal Surface Salinity Perturbations of the Meridional Overturning and Heat Transport in a Global Ocean General Circulation Model, J. Phys. Oceanogr., 38, 2739–2754, doi:10.1175/2008JPO3875.1, 2008. 3196
Stammer, D.: Global Characteristics of Ocean Variability Estimated from Regional TOPOX/POSEIDON Altimeter Measurements, J. Phys. Oceanogr., 27, 1743–1769, 1997. 3195

OSD
9, 3191–3238, 2012

Stommel, H.: Thermohaline convection with two stable regimes of flow, Tellus, 13, 224–241, 1961. 3200
Williams, R. G., Wilson, C., and Hughes, C. W.: Ocean and Atmosphere Storm Tracks: The role of Eddy Vorticity Forcing, J. Phys. Oceanogr., 37, 2267–2289, 2007. 3195
Wunsch, C.: Mass and volume transport variability in an eddy-filled ocean, Nat. Geosci., 1, 165–168, 2008. 3196, 3211
Zanna, L. and Tziperman, E.: Non-normal Amplification of the Thermohaline Circulation, J. Phys. Oceanogr., 35, 1593–1605, 2005. 3196

OSD
9, 3191–3238, 2012

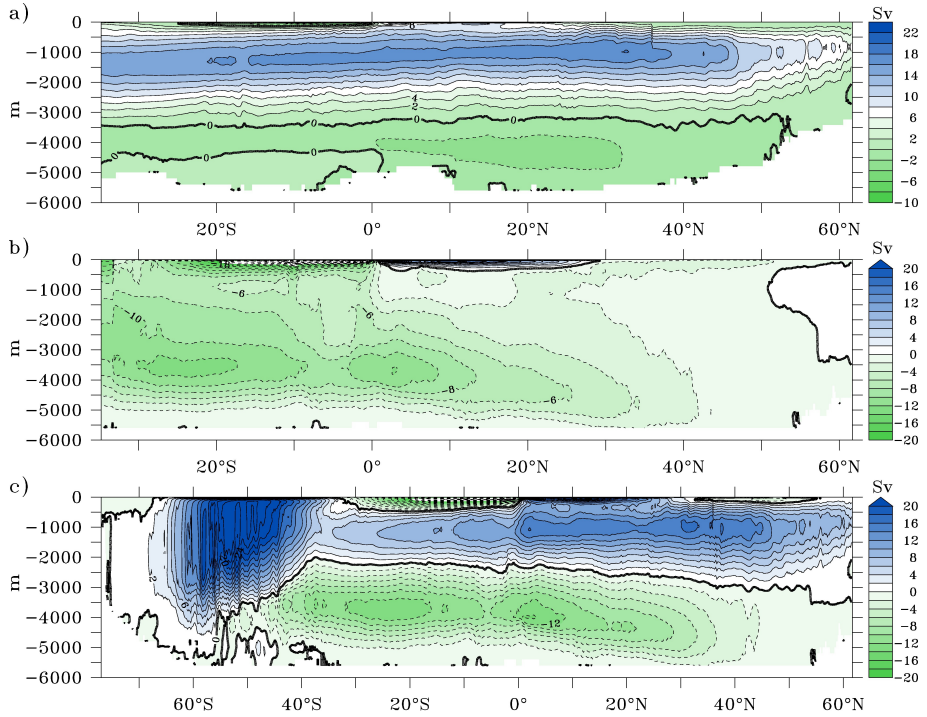

Fig. 1. Mean MOC for the 1976 to 2001 period of B025 for **(a)** the Atlantic, **(b)** the Indo-Pacific and **(c)** the global MOC. Contour interval is 2 Sv.

OSD
9, 3191–3238, 2012

Chaotic variability of the meridional overturning circulation

J. J.-M. Hirschi et al.

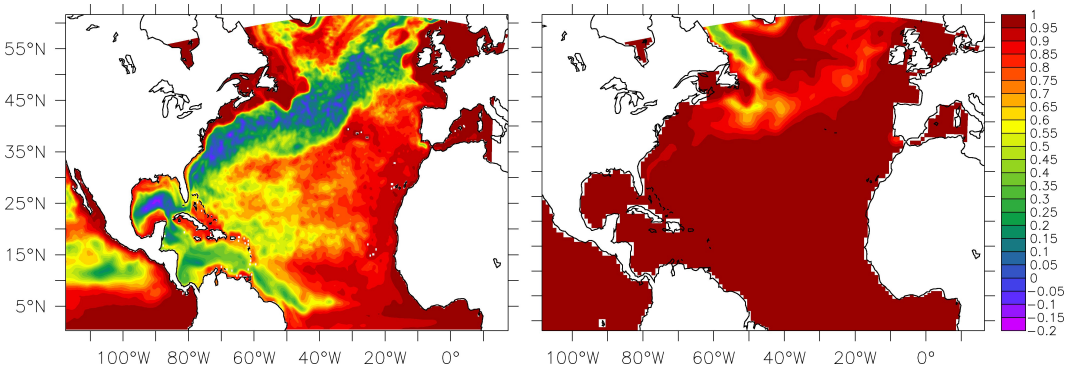

Fig. 2. Correlations between SSH variability in experiments A025 and B025 (left), and between SSH variability in A100 and B100 (right). The correlation values are obtained from 5-day averages.

OSD
9, 3191–3238, 2012

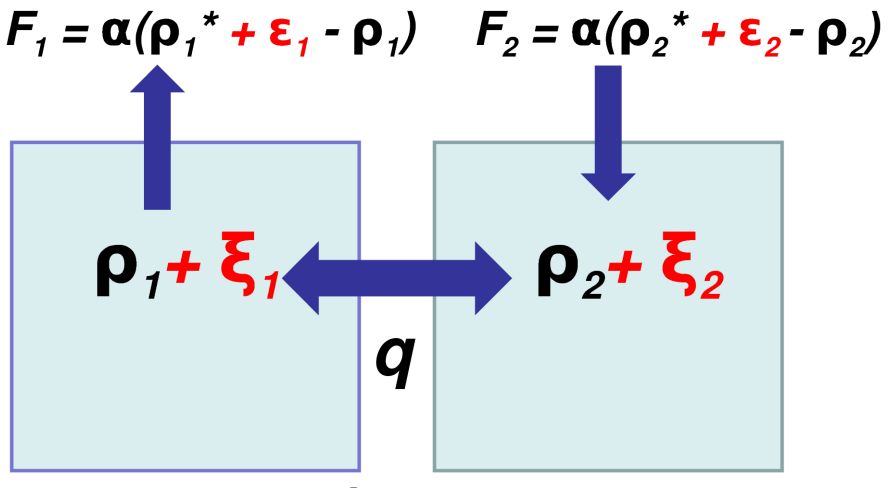

Fig. 3. Conceptual box-model used to illustrate how to extract the chaotic MOC component from the NEMO experiments. See main text for explanations.

OSD
9, 3191–3238, 2012

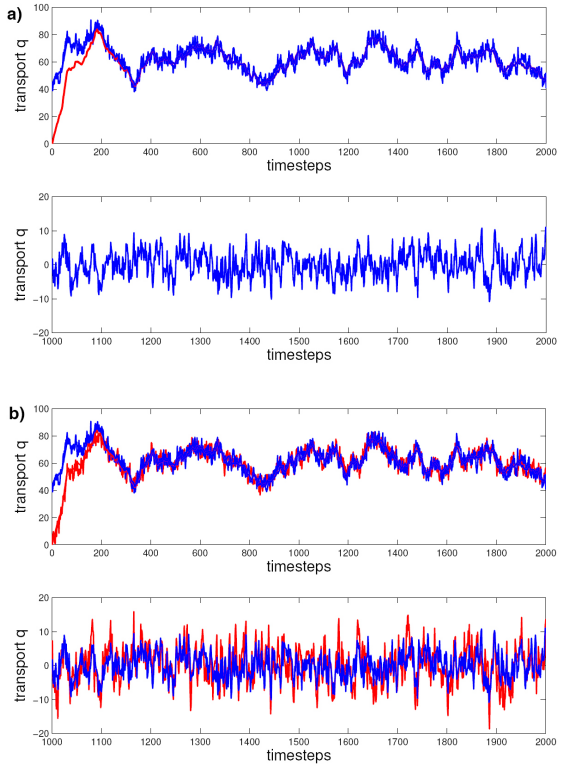

Fig. 4. Results from the conceptual model. **(a)** Top: two passes using the same surface forcing. The red line shows q for pass 1 (start from rest, no "ocean" noise). The blue line shows q for pass 2 (restart from end of pass 1, added "ocean" noise). All units are non-dimensional. Bottom: difference between passes 1 and 2 for model timesteps 1000 to 2000. **(b)** Top: same as in **(a)** but with ocean noise added to both model passes. Bottom: blue line same as in **(a)**, red line is the difference with noise added to both passes.

OSD
9, 3191–3238, 2012

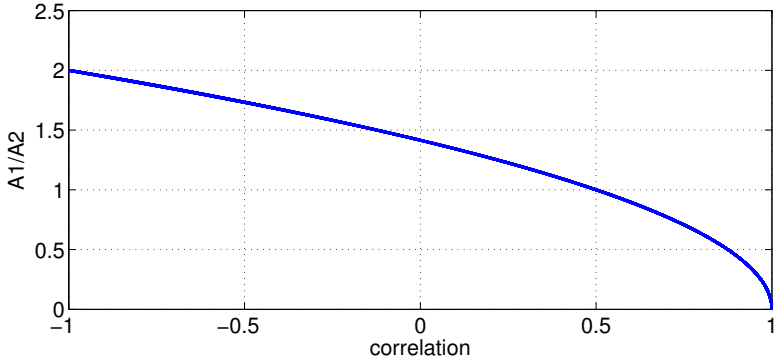

Fig. 5. Scaling factor for differences between two timeseries.

OSD
9, 3191–3238, 2012

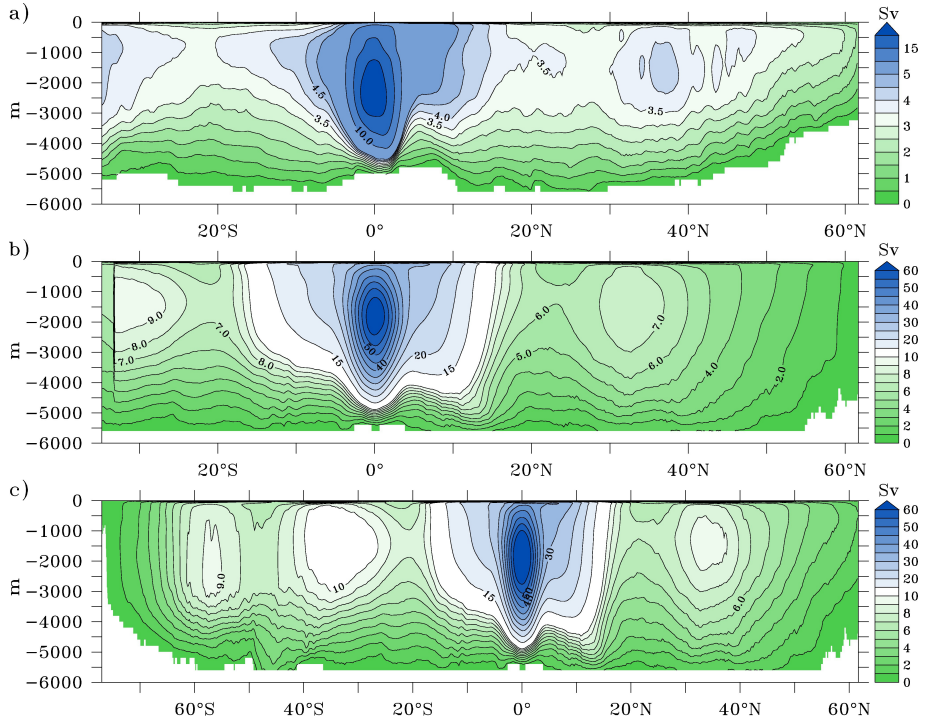

Fig. 6. Standard deviation of the MOC for the 1976 to 2001 period for experiment B025. The values are obtained from 5-day averages. **(a)** Standard deviation for the Atlantic. The contour interval is 0.5 Sv for values of up to 5 Sv. For standard deviations > 5 Sv the contour interval is 5 Sv. **(b)** As **(a)** for the Indo-Pacific. For values < 10 Sv (> 10 Sv) the contour interval 1 Sv (5 Sv). **(c)** As **(b)** for the global MOC.

OSD
9, 3191–3238, 2012

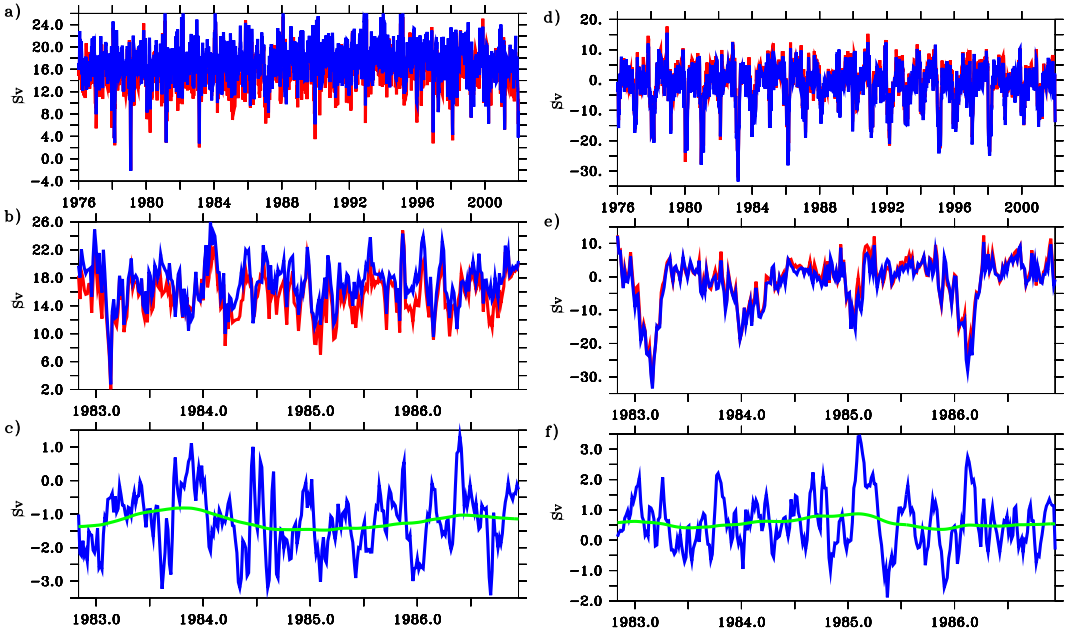

Fig. 7. MOC timeseries at 26° N for experiment A025 (blue) and B025 (red) for **(a, b, c)** the Atlantic and **(d, e, f)** Indo-Pacific. **(a, d)** 5-day MOC averages at 1000 m for 1976 to 2001. **(b, e)** zoom on the years 1983 to 1987. **(c, f)** MOC differences between A025 and B025 scaled by $1/\sqrt{2}$ as unfiltered (blue) and smoothed values. The smoothing was done using a Parzen filter with a window length of 505 days (green).

OSD
9, 3191–3238, 2012

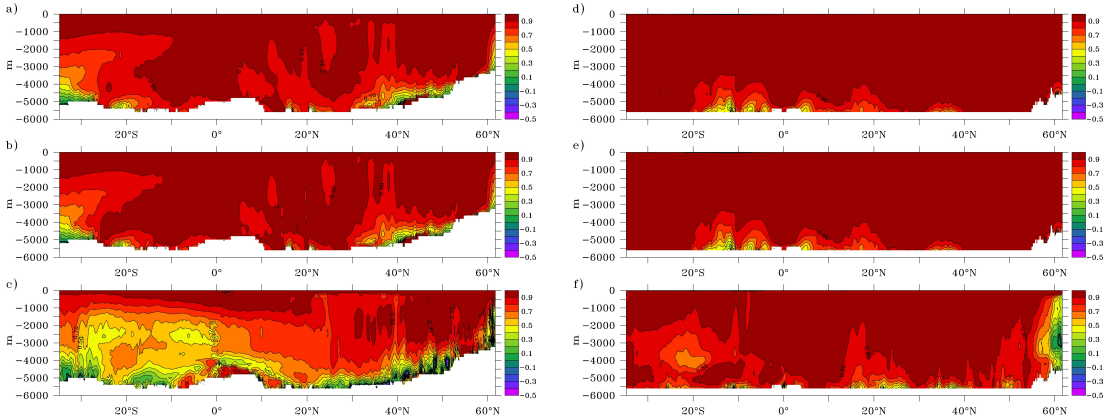

Fig. 8. Correlations between the MOC in the NEMO simulations A025 and B025 for the 1976 to 2001 period. **(a, b, c)** Correlations for the unfiltered Atlantic MOC for unfiltered (5-day averages) **(a)** subannual **(b)** and interannual **(c)** MOC variability. **(d, e, f):** As panels **(a, b, c)** but for the Indo-Pacific basin.

OSD
9, 3191–3238, 2012

Chaotic variability of the meridional overturning circulation

J. J.-M. Hirschi et al.

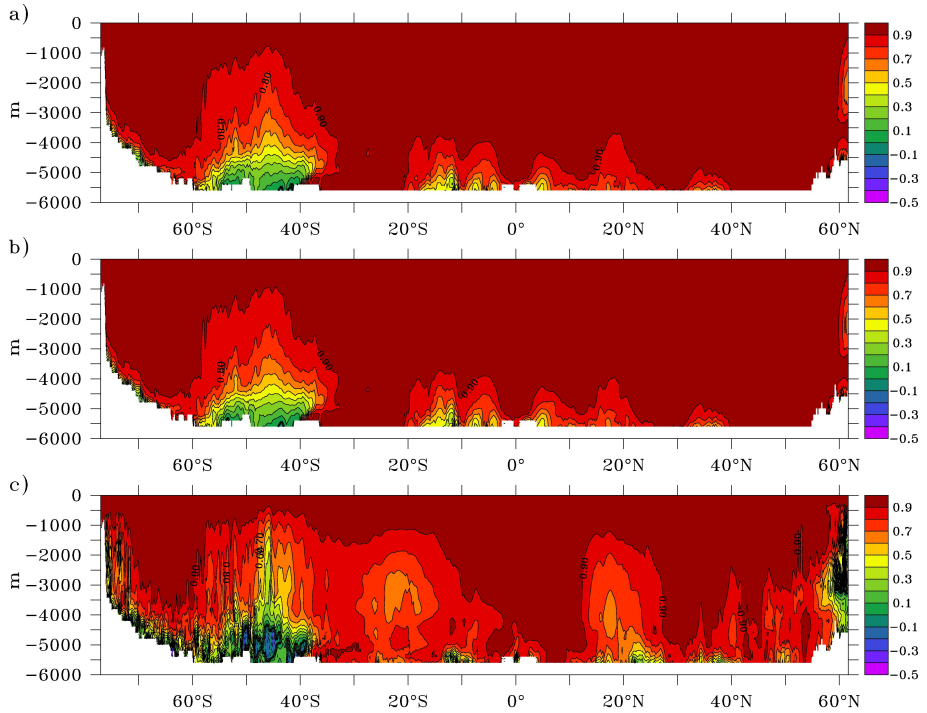

Fig. 9. As Fig. 8a, b, c but for global MOC.

OSD
9, 3191–3238, 2012

Chaotic variability of the meridional overturning circulation

J. J.-M. Hirschi et al.

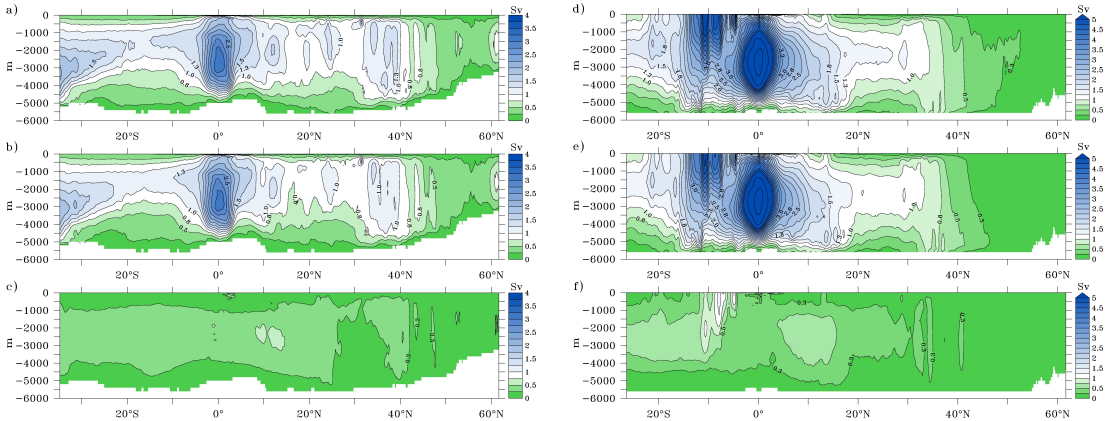

Fig. 10. Chaotic Atlantic **(a, b, c)** and Indo-Pacific **(d, e, f)** MOC variability for the eddy permitting experiments (A025, B025). **(a)** Unfiltered chaotic MOC variability (based on 5-day averages). **(b)** Subannual chaotic MOC variability. **(c)** Chaotic MOC variability on interannual timescales. **(d, e, f)** as **(a, b, c)** but for Indo-Pacific. Units are Sv and the contour interval is 0.25 Sv.

OSD
9, 3191–3238, 2012

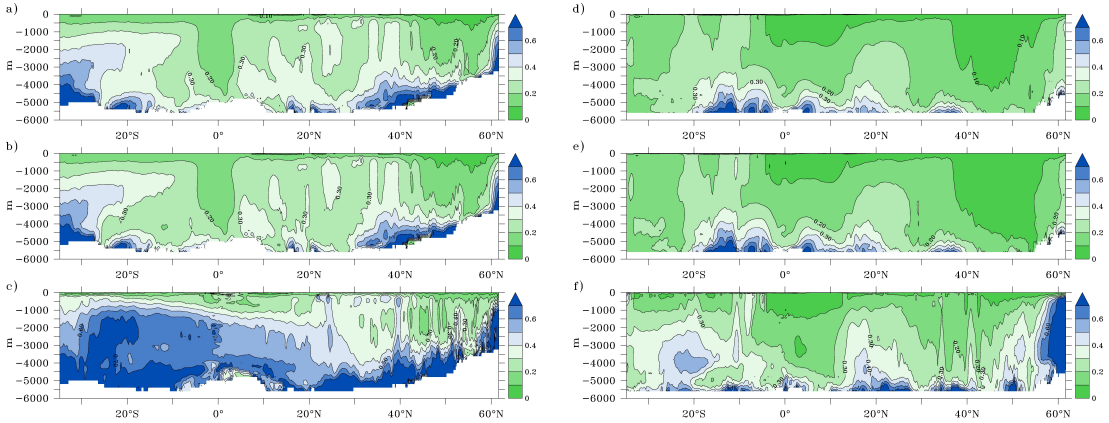

Fig. 11. Ratio between chaotic and total MOC variability for the Atlantic **(a, b, c)** and Indo-Pacific **(d, e, f)** in the eddy-permitting experiments A025, B025. **(a)** Ratio for unfiltered MOC variability (based on 5-day averages). **(b)** ratio for subannual MOC variability. **(c)** ratio for interannual MOC variability. **(d, e, f)** as a, b, c but for Indo-Pacific. The contour interval is 0.1.

OSD
9, 3191–3238, 2012

Chaotic variability of the meridional overturning circulation

J. J.-M. Hirschi et al.

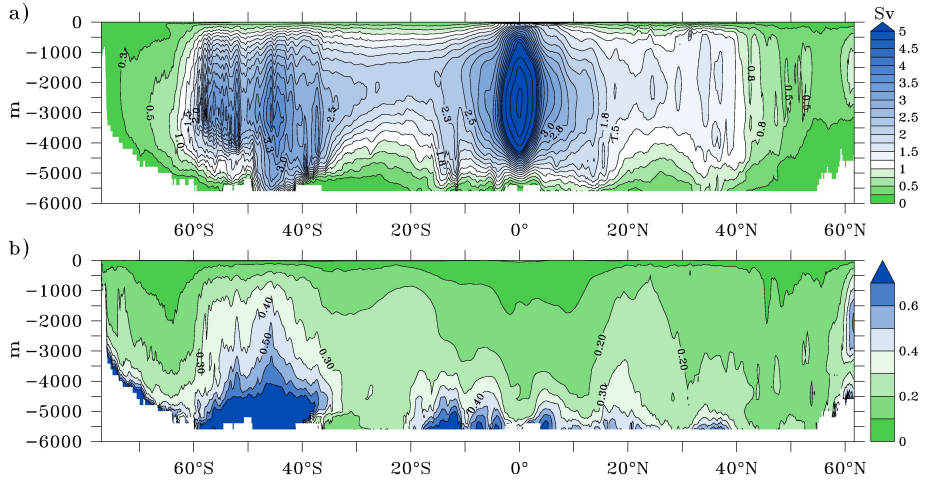

Fig. 12. (a) Unfiltered chaotic variability for global MOC. The contour interval is 0.25 Sv for values of up to 5 Sv. For values higher than 5 Sv the contour interval is 1 Sv. **(b)** Ratio between standard deviations of chaotic and total global MOC.

OSD
9, 3191–3238, 2012

Chaotic variability of the meridional overturning circulation

J. J.-M. Hirschi et al.

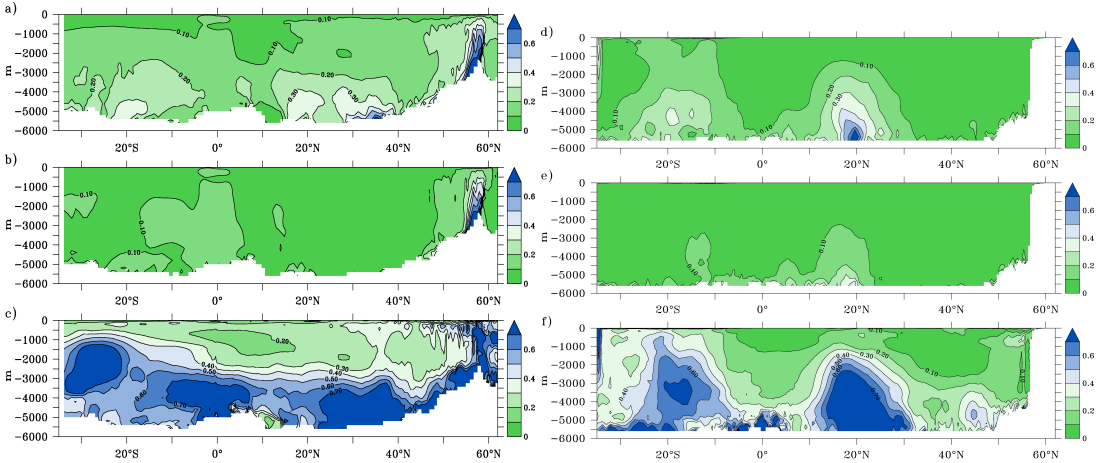

Fig. 13. Ratio between chaotic and total MOC variability for the Atlantic **(a, b, c)** and Indo-Pacific **(d, e, f)** in the non eddy-permitting experiments A100, B100. **(a)** Ratio for unfiltered MOC variability (based on 5-day averages). **(b)** ratio for subannual MOC variability. **(c)** ratio for interannual MOC variability. **(d, e, f)** as **(a, b, c)** but for Indo-Pacific. The contour interval is 0.1.

OSD
9, 3191–3238, 2012

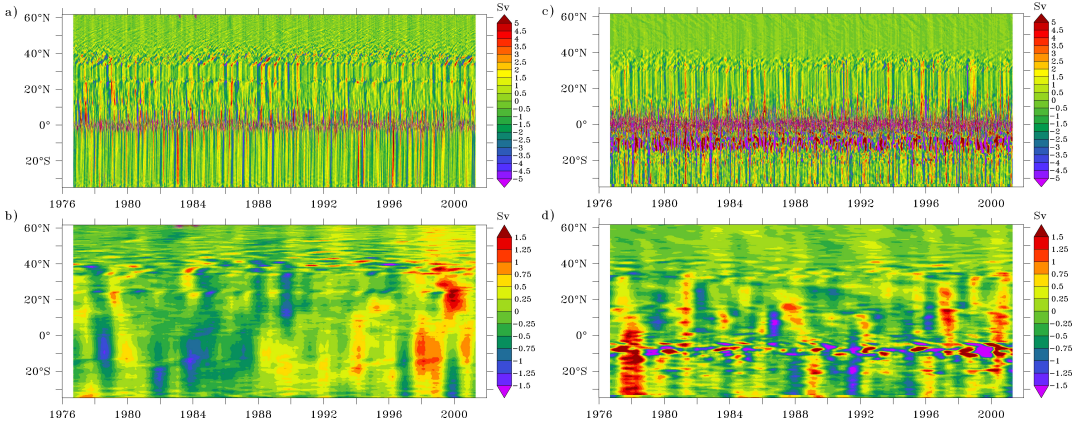

Fig. 14. Hovmöller diagram of the MOC difference between experiments A025 and B025 at 1000 m depth. **(a, b)** Chaotic Atlantic MOC variability on subannual **(a)** and interannual **(b)** timescales. **(c, d)** As panels a,b but for Indo-Pacific.

OSD
9, 3191–3238, 2012

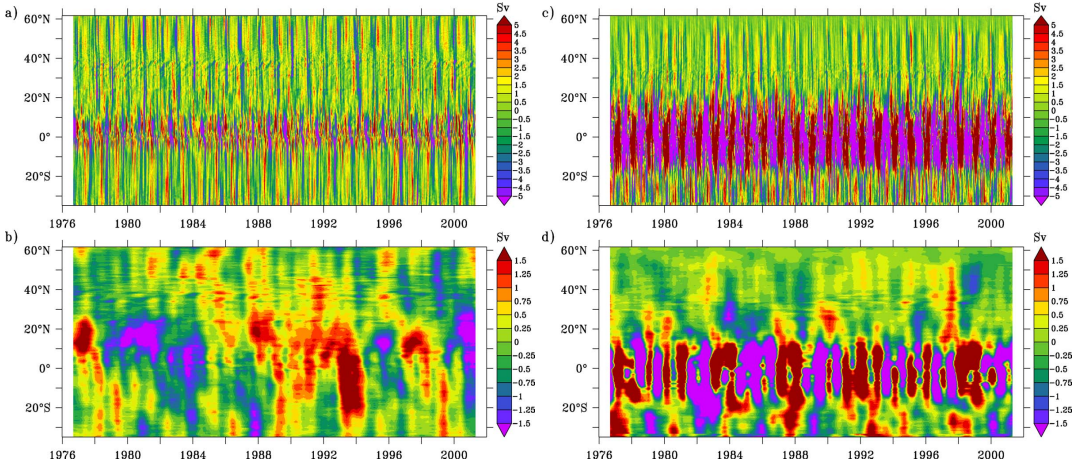

Fig. 15. Hovmöller diagram for MOC-Ekman transport at 1000 m depth for experiment B025. **(a, b)** Atlantic MOC on subannual **(a)** and interannual **(b)** timescales. **(c, d)** As **(a, b)** for Indo-Pacific.

OSD
9, 3191–3238, 2012

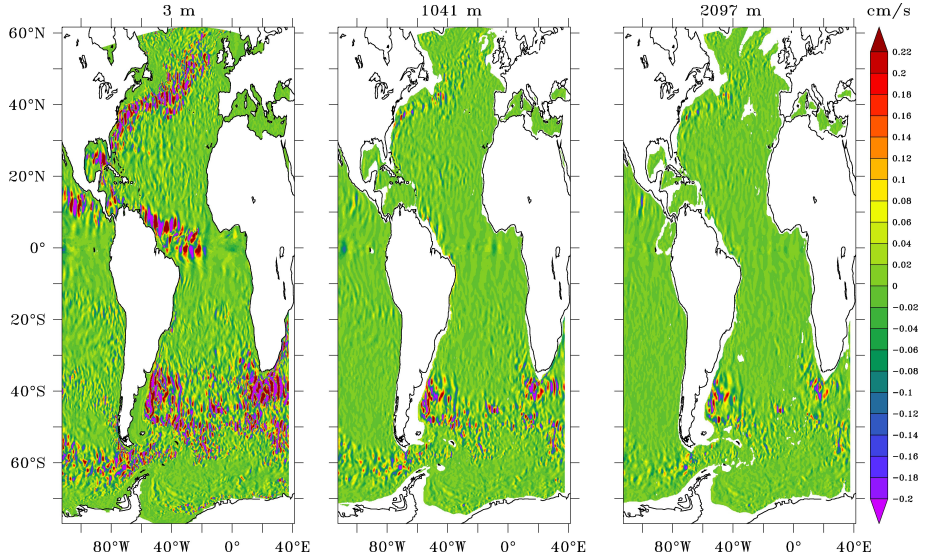

Fig. 16. Different depth ranges of mesoscale features in the North and South Atlantic. Difference between A025 and B025 for meridional velocities.

OSD
9, 3191–3238, 2012

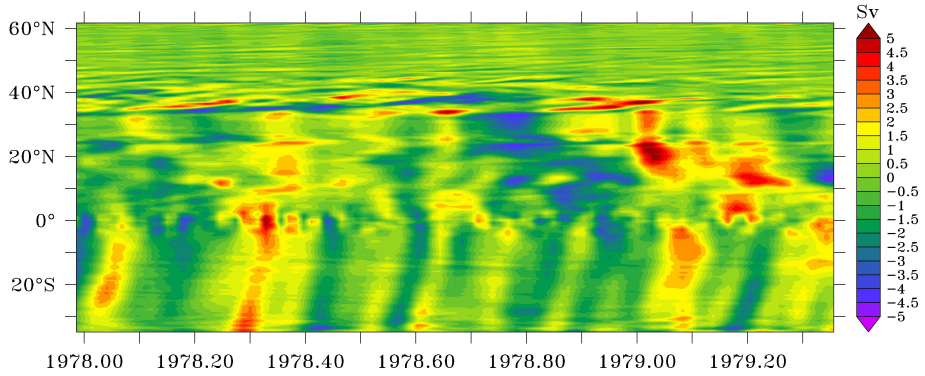

Fig. 17. Propagation of chaotic MOC anomaly fluctuations in the Atlantic at 1000 m depth (eddy-permitting case).

OSD
9, 3191–3238, 2012